Reliability analysis of pile-founded T-walls using the random variable method and random field method

Liang Zhang[1], Lei Wang[2*]

Abstract: The pile-founded walls (e.g., T-walls) are important civil infrastructure for flood protection. The stability analysis of floodwalls in the face of flooding hazards is a critical problem for the design and maintenance of floodwalls. However, most current studies for the stability assessment of floodwalls are based on deterministic analyses. The uncertainties of soil properties, which cannot be avoidable due to complex geological processes and depositional environment, are not sufficiently studied. To address the uncertainties of soil properties, a two-dimensional pile-founded T-wall system with several clay layers on the top and a sand layer on the bottom is taken as an example for the reliability analysis. Both the random variable method and random field method are adopted for the probabilistic analysis of floodwalls. The effect of the coefficient of variation (COV) and scales of fluctuation of soil properties are investigated by parametric studies. The results show that the probability of failure increases with the COV of soil properties for both methods. For the random field method, the effect of the vertical scale of fluctuation of soil properties is more profound than the horizontal scale of fluctuation. The probability of failure derived from the random variable method is generally larger than that from the random field method at high flood water elevations when the same COV of soil properties is applied. This study can provide useful references for risk-informed decision-making in the stability assessment of floodwalls in the face of flooding hazards.

Keywords: Floodwall; Reliability analysis; Spatial variability; Random field; Random variable.

[1] Research Assistant, Department of Civil and Architectural Engineering and Construction Management, University of Cincinnati, Cincinnati OH 45221, USA.

[2] Assistant Professor, Department of Civil and Architectural Engineering and Construction Management, University of Cincinnati, Cincinnati OH 45221, USA. ([*]Corresponding author: wang4li@ucmail.uc.edu)

1. Introduction

The pile-founded walls (e.g., I-walls or T-walls) play a vital role in flood protection in the New Orleans area. Since the pile-founded I-walls in New Orleans were ruined by Hurricane Katrina while pile-founded T-walls survived in several places, many studies have been performed to investigate the insufficiency of the traditional floodwall design (i.e., two-dimensional limit equilibrium analysis). Won et al. (2011) found that the complicated pile-soil interactions at deep ground layers in the pile-founded T-wall system were not fully analyzed and the unreasonable assumption of the load distribution on the battered pile in traditional design can overestimate the stability of floodwalls. The study by Hu et al. (2013) showed that the deformation of the I-wall system revealed an obvious three-dimensional effect, and the displacement of I-wall systems could not be accurately predicted by the two-dimensional analysis. Adhikari et al. (2014) indicated that the gap developed between the I-wall and the soils, and the reduced strength of the soils were the two main causes leading to the instability of floodwalls in face of the flooding hazards.

Although the failure mechanism of the pile-founded walls is considerably understood due to the pioneering work of many previous studies, most current studies are performed with deterministic analyses. However, natural soils are very complicated and highly variable geo-materials and can exhibit many uncertainties due to the natural fluctuation of material constituents and randomness in the depositional history (Huang et al. 2020). Scarce studies focused on the investigation of the effect of the uncertainties in soil properties on the stability of floodwalls, especially for pile-founded T-walls (Rajabalinejad et al. 2010; Rajabalinejad and Demirbilek 2011; Bodda et al. 2019; Davidson et al. 2020; Link 2021; Ravichandran et al. 2022). To address these uncertainties, either the random variable method (RVM) or random

field method (RFM) can be implemented for the stability analysis of the geotechnical systems (Cheng et al. 2019; Zhang et al. 2021). The random field method is a very effective approach to characterizing the spatial variability of soil properties (Jiang et al. 2014; Gong et al. 2017&2020). It has been proven to be theoretically superior to the random variable method in many scenarios (Juang et al. 2018). However, since the random field model is more complicated, additional parameters should be calibrated before the application of the random field method. It can be quite challenging to calibrate these parameters (e.g., the horizontal scale of fluctuation) in the random field method, especially when limited site investigation data can be obtained (Hicks et al. 2014), which can highly reduce the robustness of the results based on the random field method and make the simple random variable method more preferable in predicting the geotechnical system performance (Juang et al. 2018). Therefore, both the random variable method and random field method should be used for the reliability analysis of floodwalls in the face of flooding hazards.

This paper is aimed at investigating the effect of the uncertainties of soil properties, where both the random variable method and random field method are adopted for the reliability analysis of floodwalls in the face of flooding hazards. The rest of the paper is organized as follows. First, the methodologies for deterministic analysis and random field simulations are briefly introduced. Second, a baseline case for an example pile-founded T-wall system is introduced, and the reliability of the floodwall using the random variable method is analyzed. The effect of the coefficient of variation (COV) of soil properties is studied by parametric studies in this section. Third, the reliability of the example floodwall is evaluated again by using the random field method, where the influence of the COV and scales of fluctuation of soil properties is investigated. Finally, the concluding marks are summarized

based on the results represented.

2. Methodologies adopted for the reliability analysis of pile-founded T-walls

In this section, the shear strength reduction method for deterministic stability analysis and the random field simulations for probabilistic analysis are briefly introduced, respectively. Reliability analysis in terms of probability of failure, as an effective approach to quantify the uncertainties and evaluate the risk of geotechnical infrastructures such as floodwalls (Baecher and Christian 2005), is the focus of this study.

2.1 Deterministic stability analysis for pile-founded T-walls

The stability of the pile-founded T-walls can be evaluated by the equilibrium method or numerical method (USACE 2012). In this study, the 3-D explicit finite difference program FLAC3D version 7.0 (Itasca 2022) is adopted for the stability analysis of the pile-founded T-walls, where the strength reduction method is built for the evaluation. With the strength reduction method, the shear strength parameters in terms of cohesion (c) and friction angle (φ) of each soil layer are progressively reduced (or increased) by a series of values of potential factor of safety FS_i to bring the pile-founded T-wall system to a state of limiting equilibrium, which can be described as

$$c_{ri} = \frac{c}{FS_i} \tag{1a}$$

$$\tan\varphi_{ri} = \frac{\tan\varphi}{FS_i} \tag{1b}$$

where c_{ri} and φ_i are reduced cohesion and friction angle, respectively. Then the factor of safety (FS) can be used to evaluate the stability of the pile-founded T-walls.

2.2 Random field simulations of soil properties in the stability analysis for pile-founded T-walls

105 The spatial variability of soil properties is generally characterized as random fields
106 (Jiang et al. 2014; Chen et al. 2020; Hu et al. 2023). The characterization of key geotechnical
107 parameters such as unit weight, cohesion, and friction angle of soils for reliability assessment
108 is carefully selected. Since the COV of the unit weight is generally below 0.1 (Phoon and
109 Kulhawy 1999; Li et al. 2014), the unit weight is set as a constant value while the cohesion
110 and friction angle are modeled as random variables or random fields in this study. Since the
111 soil properties are non-negative, the soil properties are generally assumed as lognormally
112 distributed (Cho 2010; Jiang et al. 2014; Gong et al. 2020). The mean $\mu_{\ln s}$ and the standard
113 deviation $\sigma_{\ln s}$ of the normal random field $\ln(s)$ are computed with the given mean μ_s and the
114 coefficient of variation (COV) δ_s of the original soil property s as follows.

115 $$\sigma_{\ln s} = \sqrt{\ln(1+\delta_s^{\,2})} \tag{2a}$$

116 $$\mu_{\ln s} = \ln(\mu) - 0.5\sigma_{\ln s}^2 \tag{2b}$$

117 The anisotropic exponential autocorrelation structure is selected to characterize the
118 correlation coefficient ρ_{ij} between the soil property s at two different locations of (x_i, y_i) and
119 (x_j, y_j), which is calculated as follows.

120 $$\rho_{ij} = \rho(|x_j - x_i|, |y_j - y_i|) = \exp(-\frac{2|x_j - x_i|}{\lambda_x} - \frac{2|y_j - y_i|}{\lambda_y}) \tag{3}$$

121 where $|x_j - x_i|$ and $|y_j - y_i|$ represent the absolute distances between the two positions of (x_i, y_i)
122 and (x_j, y_j) along the X and Y directions, namely, the horizontal and vertical directions,
123 respectively; whereas, λ_x and λ_y are the horizontal and vertical scales of fluctuation of the
124 equivalent normal random field $\ln(s)$ along the X and Y directions, respectively.

125 Since a fixed value is mapped to the soil element domain rather than at the mesh grids,

the average effect over the soil element domain should be considered. The mean of soil property $\mu_{\ln sE}$ that is averaged over each soil element domain is equal to that of the local soil property $\mu_{\ln s}$ while the standard deviation of the averaged soil property $\sigma_{\ln sE}$ is decreased. Based on the autocorrelation structure built in Eq. (3), the locally averaged mean $\mu_{\ln sE}$ and standard deviation $\sigma_{\ln sE}$ over a rectangular mesh with side length l_x and l_y can be derived as (Knabe et al. 1998; Huang and Griffiths 2015):

$$\sigma_{\ln sE}^2 = \sigma_{\ln s}^2 \gamma(l_x, l_y) \tag{4a}$$

$$\mu_{\ln sE} = \mu_{\ln s} \tag{4b}$$

$$\gamma(l_x, l_y) = \frac{4}{l_x^2 \cdot l_y^2} \int_0^{l_y} \int_0^{l_x} (l_x - \tau_x)(l_y - \tau_y) \exp\left(-\frac{2|\tau_x|}{\lambda_x} - \frac{2|\tau_y|}{\lambda_y}\right) d\tau_x d\tau_y \tag{4c}$$

The locally averaged $\mu_{\ln sE}$ and $\sigma_{\ln sE}$ are involved in the following random field simulations instead of $\mu_{\ln s}$ and $\sigma_{\ln s}$. A variety of methods for random field generations can be available now, such as the local average subdivision method, turning-band method, fast Fourier transformation method, and covariance matrix decomposition method (Fenton 1994; Wang et al. 2020; Gong et al. 2021). As a common and easy-to-implement method, the covariance matrix decomposition method is adopted for the random field generation in this study. With the prior knowledge of the mean, standard deviation, and autocorrelation structure, the $n_E \times n_E$ autocorrelation matrix $\boldsymbol{R}_{\ln s}$ of the soil property between each two soil elements can be established. One random field simulation can be generated as follows.

$$s_{ij} = \exp\left(\mu_{\ln sEj} + \sigma_{\ln sEj} \cdot \ln s_{ij}\right) \tag{5}$$

where s_{ij} is the j^{th} numerical element of the i^{th} realization of the random field (i = 1, 2, …, N_p; j = 1, 2, …, n_E), in which N_p is the number of realizations of the random field and n_E is the

number of discretized numerical elements; $\mu_{\ln sEj}$ and $\sigma_{\ln sEj}$ are the averaged mean and standard deviation of the soil property ln(s) over the j^{th} numerical element, respectively; $\ln s_{ij}$ is the j^{th} element of the i^{th} realization of the random field. The matrix $\ln s_i$ of the soil property for all the numerical elements is derived as follows.

$$\ln \boldsymbol{s}_i = \boldsymbol{L}_{\ln s} \boldsymbol{\xi}_i \tag{6a}$$

$$\boldsymbol{R}_{\ln s} = \boldsymbol{L}_{\ln s} \times \boldsymbol{L}_{\ln s}^{T} \tag{6b}$$

where $\boldsymbol{\xi}_i$ is an $n_{\text{E}} \times 1$ standard normal sample vector (i = 1, 2, …, N_p), which is sampled by the subdomain method described later; $\boldsymbol{L}_{\ln s}$ is a lower triangular matrix of autocorrelation matrix $\boldsymbol{R}_{\ln s}$ derived by the Cholesky decomposition technique.

2.3 Modified subdomain sampling method for the random field simulations of soil properties

Monte Carlo simulations (MCS) have been widely used for the random field simulations of soil properties. However, the MCS could be computationally challenging for the low probability scenarios (e.g., the flood water elevation for the pile-founded T-wall is low) (Jiang and Huang 2016; Gao et. 2019). With the advance in computational science and the pioneering work of previous studies, some strategies have been proposed to improve computational efficiency, such as the parallel computing method (Spencer 2007), the Latin hypercube sampling (LHS) (Lo and Leung 2017), subset sampling method (Wang et al. 2010; Au and Wang 2014), and subdomain sampling method (SSM) (Juang et al. 2017; Gong et al. 2020). The subdomain sampling method exhibits high efficiency and accuracy to derive the probability of failure in face of small probability events (Juang et al. 2017). Some SSM-based practical designs have been conducted in previous studies (e.g., Gong et al. 2020; Yun et al.

169 2020). The original SSM is modified to further enhance the computational efficiency in the
170 estimate of the low failure probabilities in this study.

171 In the original SSM, the possible domain of input uncertain variables is discretized
172 into a series of continuous subdomains. Then a distance index (d) is used to partition the
173 domain based on Hasofer–Lind reliability index (Hasofer and Lind 1974), which is
174 formulated as

175 $$d = \sqrt{[u]^T [R][u]} \tag{7}$$

176 where $u = [u_1, u_2, u_3, \ldots, u_n]^{\mathrm{T}}$ is a vector of transformed standard normal variables from the
177 original space of the input parameters and n is the number of input uncertain variables X; R is
178 the correlation matrix among the standard normal variables u. The relations between the
179 component u_i of u and component x_i of the X are described as

180 $$u_i = \Phi^{-1}(F(x_i)) \tag{8}$$

181 where $F(x_i)$ is the cumulative distribution function (CDF) of uncertain variable x_i; the $\Phi(\cdot)$ is
182 the CDF of the standard normal variables. As such, the domain of input uncertain variables
183 can be partitioned into a series of subdomains [0, d_1), [d_1, d_2), [d_2, d_3), etc. With the sampled
184 domain [0, d_{max}), d^2 follows the chi-square distribution with n degree of freedom. The
185 possibility of the samples located in and outside this domain is (1-ε) and ε, which can be
186 described as

187 $$\chi_n^2(d_{\max}^2) = \varepsilon \tag{9}$$

188 where $\chi_n^2(\cdot)$ is the chi-square CDF with n degrees of freedom. Then the probability of each
189 subdomain can be calculated as

190 $$p_{A_i} = \Pr[d_{i-1}^2 \le [u]^T [R][u] < d_i^2] = \chi_n^2(d_i^2) - \chi_n^2(d_{i-1}^2) = q^i \tag{10}$$

According to previous studies, the q is generally no large than 1/2 (i.e., $q \leq 1/2$) (Gong et al. 2016&2020; Juang et al. 2017), and $q = 1/3$ is adopted in this study following Gong et al. (2020). The detailed procedures for generating samples in each subdomain can be referred to Gong et al. (2016). With generated samples, the conditional failure probability p_{fi} in the subdomain $[d_{i\text{-}1}, d_i)$ is calculated as

$$p_{fi} = \frac{t_{fi}}{t} \tag{11}$$

where t is the total number of samples generated in the subdomain $[d_{i\text{-}1}, d_i)$ and t_{fi} is the number of failure samples in this subdomain. The COV of the conditional failure probability $\delta_{P_{fi}}$ can be estimated in the subdomain as

$$\delta_{P_{fi}} \approx \sqrt{\frac{1\text{-}p_{fi}}{t \cdot p_{fi}}} \tag{12}$$

The total probability of failure P_f can be obtained by the summation of all the conditional probabilities of failure, which can be calculated as

$$P_f = \sum_{i=1}^{ns} (p_{A_i} \cdot p_{f_i}) \tag{13}$$

where ns is the total number of subdomains. The COV of P_f can be calculated as

$$\delta_{P_f} \approx \frac{\sqrt{\sum_{i=1}^{n_s} [p_{A_i}^2 \cdot (p_{fi} \cdot \delta_{p_{fi}})^2]}}{\sum_{i=1}^{n_s} (p_{A_i} \cdot p_{fi})} = \frac{\sqrt{(1/t) \cdot \sum_{i=1}^{n_s} [p_{A_i}^2 \cdot p_{fi} \cdot (1 - p_{fi})]}}{\sum_{i=1}^{n_s} (p_{A_i} \cdot p_{fi})} \tag{14}$$

To implement the SSM, the number of samples t in each subdomain and the total number of subdomains ns should be determined first. Herein, $t = 30$ is selected by the trade-off between the computational efficiency and variation of P_f (Juang et al. 2017; Gong et al. 2020). In the original subdomain sampling method (SSM), the number (ns) of subdomains

can be determined by the following equation after the target probability of failure P_f is estimated:

$$\frac{q^{ns}}{P_f} \le 0.01 \tag{15}$$

However, a fixed total number of $t \times ns$ simulations will be performed for either a high or low probability of failure, resulting in unnecessary computation for the high probability of failure, since smaller domains can be sufficient for the estimate of a high probability of failure. Therefore, Yun et al. (2020) suggested that the ns can be adaptively adjusted by the 5% error for the probability of failure from the first k ($k \le ns$) subdomains (see Eq. (16)). As shown in Eqs. (16-18), the two conditions from the original SSM and Yun et al. (2020) can be reached by a stricter criterion but with a simpler form that is easy to implement for programming. Therefore, the first strategy to enhance computational efficiency is achieved to adaptively determine the number of the subdomains in the modified SSM (see Eq. (18)).

$$\sum_{i=k+1}^{ns} p_{A_i} \cdot p_{fi} < \sum_{i=k+1}^{ns} p_{A_i} = \frac{q^{k+1}(1-q^{ns-k})}{1-q} < \frac{q^{k+1}}{1-q} < \frac{q^{k+1}}{q} = q^k \tag{16a}$$

$$\varepsilon_r^{(k)} = \frac{P_f - P_f^{(k)}}{P_f} = \frac{\sum_{i=k+1}^{ns} p_{A_i} \cdot p_{fi}}{\sum_{i=1}^{k} p_{A_i} \cdot p_{fi} + \sum_{i=k+1}^{ns} p_{A_i} \cdot p_{fi}} < \frac{\sum_{i=k+1}^{ns} p_{A_i} \cdot p_{fi}}{\sum_{i=1}^{k} p_{A_i} \cdot p_{fi}} < \frac{q^k}{\sum_{i=1}^{k} p_{A_i} \cdot p_{fi}} \tag{16b}$$

$$\frac{q^{ns}}{P_f} = \frac{q^{ns}}{\sum_{i=1}^{k} p_{A_i} \cdot p_{fi} + \sum_{i=k+1}^{ns} p_{A_i} \cdot p_{fi}} < \frac{q^{ns}}{\sum_{i=1}^{k} p_{A_i} \cdot p_{fi}} < \frac{q^k}{\sum_{i=1}^{k} p_{A_i} \cdot p_{fi}} < 0.01 \tag{17}$$

$$\frac{q^k}{\sum_{i=1}^{k} p_{A_i} \cdot p_{fi}} < 0.01 \tag{18}$$

The second strategy for the modification of the original SSM is without searching for FS by

following Huang et al. (2017), which means the exact *FS* is not calculated in this case. Instead, whether the pile-founded T-wall system is stable or unstable is judged by substituting *FS* = 1.0 in the strength reduction method with only one trial calculation. With all the strategies applied in the modified SSM, the modified SSM is approximately 7~9 times more efficient in terms of computational time than the original SSM for all the cases involved.

3. Reliability analysis of floodwalls using the random variable method

In this section, the reliability analysis of floodwalls is performed using the random variable method. The baseline case for a pile-founded T-wall system is first analyzed to investigate the influence of the flood water elevation on the probability of failure of the floodwall. The effect of the COV of the soil properties is also investigated for the reliability analysis of the floodwall.

3.1 Results analysis for the baseline case using the random variable method

To investigate the influence of flood water elevations on the probability of failure, a two-dimensional pile-founded T-wall system modified from Won et al. (2011) is studied, where the thin layers with similar strength soil properties are combined into thick layers and the sheet pile is removed to reduce the computational burden and simplify the procedures to perform the parametric study. Therefore, the model in this study has similar complexity to the exquisite model in Won et al. (2011) and is sufficiently realistic and meaningful, which ensures the derived conclusions from the modified model show engineering significance and can provide useful guidance for reliability-based floodwall designs. Figure 1 shows the geometry parameters of the pile-founded T-wall system. The floodwall system consists of an earth levee, a concrete T-wall, and three rows of H-piles (HP 14×73). The earth levee with a

height of 1 m and slope of 3H:1V is on the top of the T-wall base. The T-wall with a height of 5.15 m and a base of 4.0 m is supported by the three rows of batter H-piles. The top elevation of the T-wall is EL. +3.65 m while the bottom elevation of the T-wall is EL. -1.5 m. Three rows of H-piles are inclined with the same ratio of 1H:3V to the vertical plane. The mesh of the built numerical model is presented in Figure 2. As shown in Figure 2, five soil layers are configured in this pile-founded T-wall system. Four clay layers (i.e., the levee fill, the peat, the soft clay, and the hard clay) are at the top and a sand layer is located at the bottom. The top elevation and soil properties of each soil layer for deterministic analysis are tabulated in Table 1. The H-piles are embedded in the sand layer to guarantee enough capacity for the floodwall.

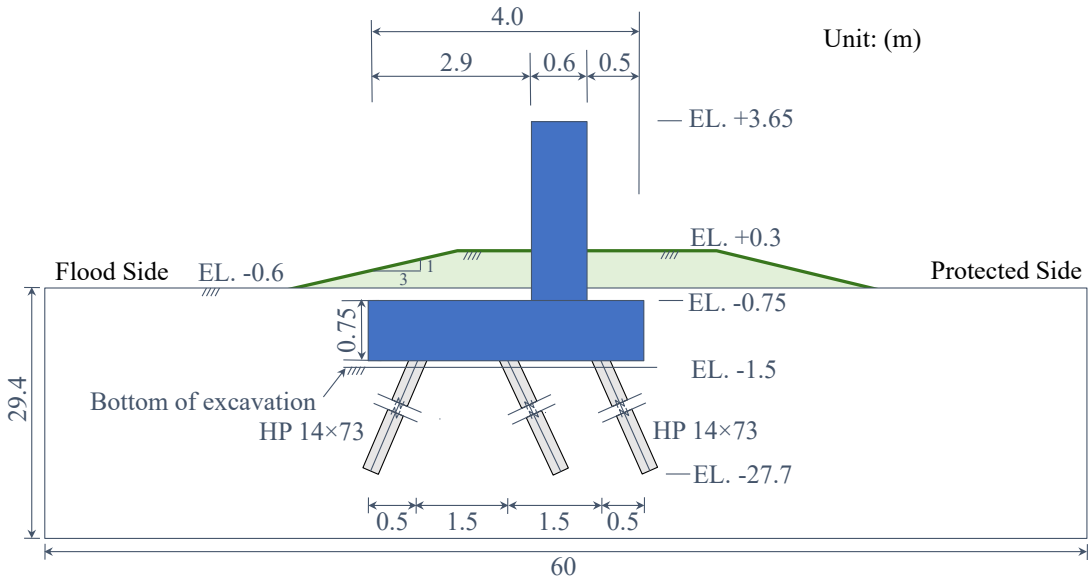

Figure 1. Illustration of the geometry of pile-founded T-wall system (after Won et al. 2011)

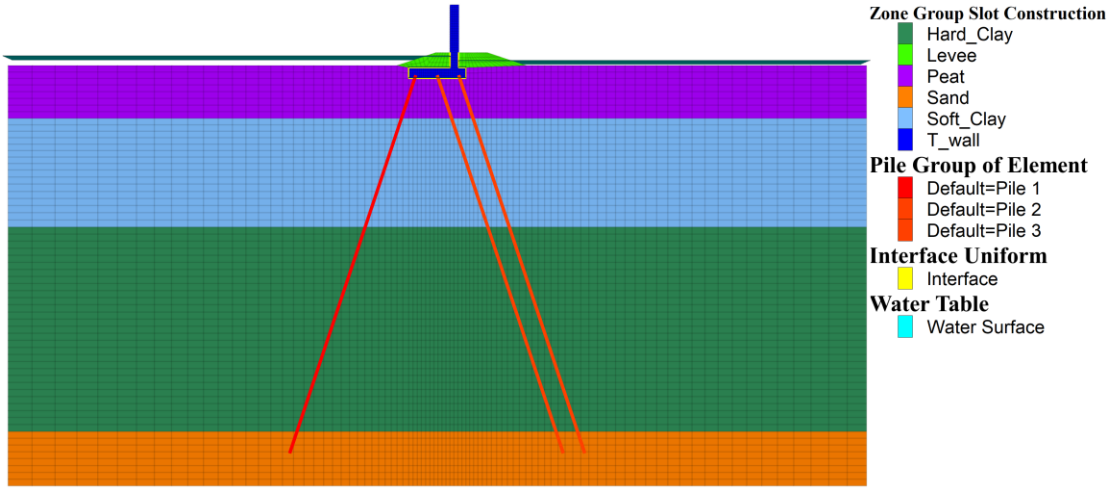

Figure 2. Mesh of pile-founded T-wall system for the numerical simulations

Table 1. Soil properties adopted in the deterministic analysis

Layer	Soil type	Top elevation (m)	c_u (kPa)	φ (°)	γ (kN/m^3)	G (kPa)	K (kPa)
Levee fill	Clay soil	0.3	23.9	-	17.3	3585	8.86e4
Peat	Clay soil	-0.6	5.7	-	12.6	574.6	1.42e4
Soft Clay	Clay soil	-4.3	7.2	-	15.7	933.7	2.30e4
Hard Clay	Clay soil	-11.9	9.6	-	15.7	2863.2	7.09e4
Sand	Sand soil	-26.2	-	30	18.1	7804.4	1.69e4

In the numerical simulations with FLAC3D version 7.0, the Mohr-Coulomb model is used to model the behavior of all soil layers. The T-wall is simulated by the brick elements with elastic behavior, and the interactions between the T-wall and the soil are modeled by the interface elements in FLAC3D. Interface elements are attached to the T-wall surface through the interface nodes in the numerical simulations. The elastic-perfectly-plastic model is adopted for the behavior of the interface to characterize the sliding and gap between the soil and T-wall. The shear strength parameters cohesion and friction angle of the interface are set following Won et al. (2011). The shear stiffness k_s and normal stiffness k_n for deformation are

276 determined as follows (Itasca 2022):

277 $$ks \approx kn \approx 10 \cdot [\frac{(K + 4/3G)}{\Delta z_{min}}] \quad (19)$$

278 Where Δz_{min} is the smallest width with of an adjoining zone in the normal direction. K and G
279 are the bulk modulus and shear modulus of the soil, respectively. The H-piles are modeled by
280 the pile elements to consider the support for the floodwall. The detailed structure properties
281 and the interface properties adopted in the numerical simulations can be referred to Won et al.
282 (2011). The T-wall and H-piles are connected by the end bearing spring. The connection is
283 assumed to be a continuously reinforced concrete and the properties for the end bearing spring
284 are also set following Won et al. (2011). The horizontal displacement of the four side
285 boundary planes of the model is restricted in the normal direction, and the displacement at the
286 base of the model is fixed. To investigate the stability of the pile-founded floodwall with
287 different flood water elevations, initial stress and strain for the numerical model without any
288 geotechnical structures (i.e., the T-wall, and H-piles) are first computed. Then the T-wall and
289 H-piles are built to update the stress and strain before the pore water pressure is applied to the
290 flood protection system. The initial water table elevation is set as EL. -0.3 m in protect side
291 and the initial flood water elevation is set as EL. +0 m in the flood side. Finally, the flood
292 water elevation increases in an increment of 0.2 m from EL +0 m to EL +3.6 m on the flood
293 side (i.e., the left side of the model). The critical mechanism of the floodwall (consisting of
294 soils, T-wall, and H-piles) with flood water elevations for potential failure modes is validated
295 based on the study by Won et al. (2011).

296 The soil properties adopted for the probabilistic analysis using the random variable
297 method are summarized in Table 2. Since the undrained condition is applied in this example,

298 the undrained shear strength c_u is modeled as a random variable for the clay layers while the
299 friction angle φ is taken as a random variable for the sand layer. The remaining soil properties
300 are set as constant values. Note that the soil strength properties are assumed as lognormally
301 distributed. The mean of c_u and φ of each soil layer is the same as that from deterministic
302 analysis (see Table 1). According to previous studies, the COV of clay typically ranges from
303 0.1 to 0.5 while the COV of sand typically varies from 0.05 to 0.15 (Phoon and Kulhawy
304 1999; Alamanis 2017; Wu et al. 2019; Ma et al. 2022). The midpoints of these ranges are
305 selected for the baseline to show a "general case" scenario. The maximum and minimum of
306 these ranges are adopted for "best case" and "worst case" scenarios in the following
307 parametric study. As such, the effect of uncertainties in soil properties on the reliability of
308 floodwall can be revealed in this study. Therefore, the COV of c_u for clay layers is set as 0.3
309 and the COV of φ for the sand layer is set as 0.1 in the baseline. The modified SSM is adopted
310 for the calculation of the probability of failure. The probability of failure with different flood
311 water elevations is illustrated in Figure 3. As shown in Figure 3, the probability of failure P_f
312 stably increases first and then rapidly increases with the flood water elevation. The largest P_f
313 will be obtained when the flood water elevation approaches the T-wall top (i.e., EL. +3.6 m),
314 which is mainly owing to the increase of the pore water pressure and load effect triggered by
315 the water weight with the flood water elevation. The pore pressure reduces the effective stress
316 of the soils and leads to more possibility of failure in the soil layers. The water weight load
317 normally distributed on the T-wall and the earth levee on the flood side results in the slide and
318 rotation of the floodwall system as a whole.
319
320 Table 2. Soil properties adopted for the baseline case in the probabilistic analysis

Soil type	Clay soil	Sand soil
Soil properties	Undrained shear strength, c_u (kPa)	Friction angle, φ (°)
Probability distribution	Lognormal	Lognormal
Mean	See Table 1	See Table 1
Coefficient of variation	0.3	0.1
Horizontal scale of fluctuation for RFM, λ_x (m)	50	40
Vertical scale of fluctuation for RFM, λ_y (m)	4	2

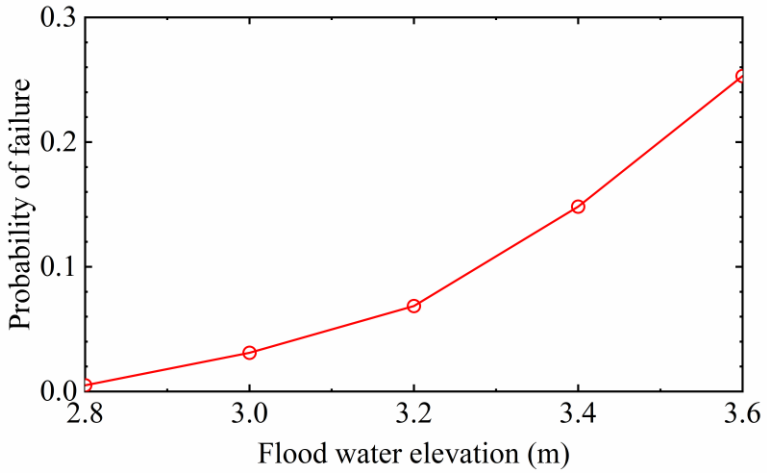

Figure 3. Effect of the flood water elevation on the probability of failure of the floodwall using random variable method

3.2 Effect of the COV of soil properties on the reliability of the floodwall

To further investigate the effect of the COV of the soil properties, a parametric study is performed for the reliability analysis of the floodwall. The probabilistic case from section 3.1 is taken as a baseline case. Figure 4 shows the influence of the COV of c_u of the clay layers on the probability of failure of the floodwall. The probability of failure increases with the COV of c_u,, which implies that more uncertainties in the strength property of clay layers will make the floodwall system more likely to fail. Similar results for the different COV of φ of the strength property for sand can also be obtained in Figure 5. Figure 5 also shows that the probability of failure with flood water elevations for the COV of the strength property for

sand equal to 5% is similar to that for the COV equal to 10%. It is possible because the two curves are at a similarly low level of uncertainty and the COV of the strength property for sand is not changed too much. As the COV of the strength property for sand increases from 10% to 15%, the effect of the COV becomes much more significant due to the nonlinear relationship between the probability of failure of the floodwall and the COV of the strength property for sand. The general trend is captured to show that the probability of failure of the floodwall increases with the COV of soil strength properties. The stability of the floodwall mainly depends on the soil-bearing capacity and the support of the structures (i.e., the T-wall and the H-piles). The end-bearing capacity of the H-piles largely depends on the soil properties around the pile tip. Therefore, the COV of strength properties for both clay and sand layers will cause a huge effect on the stability of the floodwall system, although it seems that the slip surface does not go through the sand layer. However, the probability of failure can be varied with the COV of the strength property for clay at both low and high flood water elevations. By contrast, the COV of the strength property for sand is more influential at high flood water elevations and results in a higher probability of failure than that from the COV of the strength property for clay at high flood water elevations. This can be explained by the fact that the strength of the soil layers can considerably resist flooding hazards with relatively small deformation at low flood water elevations and the support of the structures becomes more crucial with the increase of the flood water elevation. Therefore, the COV of the strength property for clay can be influential on the probability of failure for all the flood water elevations while the probability of failure is less sensitive to the COV of the strength property for sand at low flood water elevations.

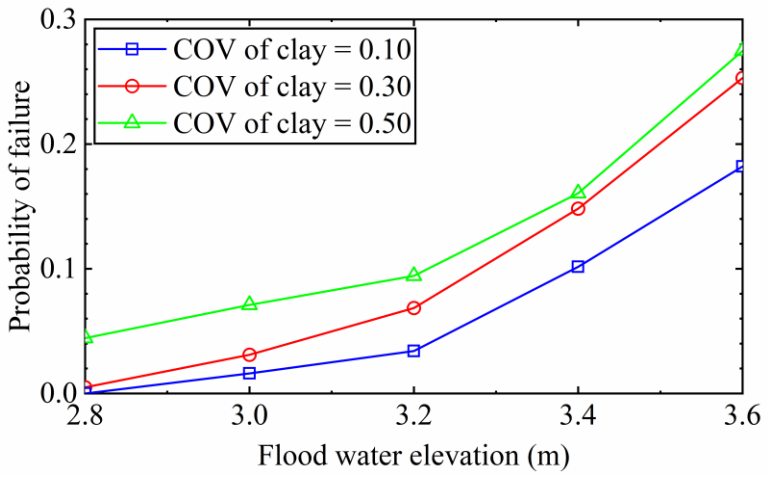

Figure 4. Effect of COV of the strength property of clay layers on the probability of failure of the floodwall using random variable method

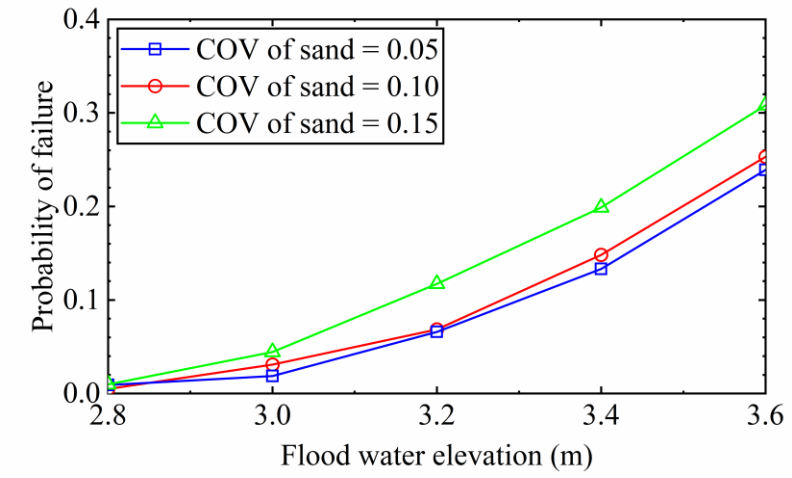

Figure 5. Effect of COV of the strength property of sand layer on the probability of failure of the floodwall using random variable method

4. Reliability analysis of floodwalls using random field method

In this section, the reliability of the pile-founded floodwall with different flood water

elevations is analyzed again using the random field method. The baseline case is first studied as a basic model for reliability analysis. Then parametric studies are performed to investigate the effect of the COV and scales of fluctuation of the soil properties on the probability of failure of the floodwall.

4.1 Results analysis for the baseline case using the random field method

To consider the effect of the spatial variability of the soil properties, the baseline case using the random field method is studied first. The statistics of the soil properties are taken the same as that from the random variable method (see Table 2). Compared to the random variable method, additional horizontal and vertical scales of fluctuation λ_x and λ_y should be determined. The horizontal scale of fluctuation λ_x typically ranges from 10 to 92.4 m and the vertical scale of fluctuation λ_y typically ranges from 0.1 to 8.0 m for clay soil while the λ_x and λ_y for sand soil fall within the range from 12.7 to 75 m and from 0.14 to 3.0 m, respectively (Phoon and Kulhawy 1999; Li et al. 2015). Therefore, the λ_x is set as 50 m and λ_y is set as 4 m for clay soil while the λ_x is set as 40 m and λ_y is set as 2 m for sand soil (see Table 2) in the baseline to show a "general case" scenario. The probability of failure with different flood water elevations is plotted in Figure 6. The probability of failure increases with the flood water elevation due to the increased pore water pressure and water weight load, which is similar to the results from the random variable method.

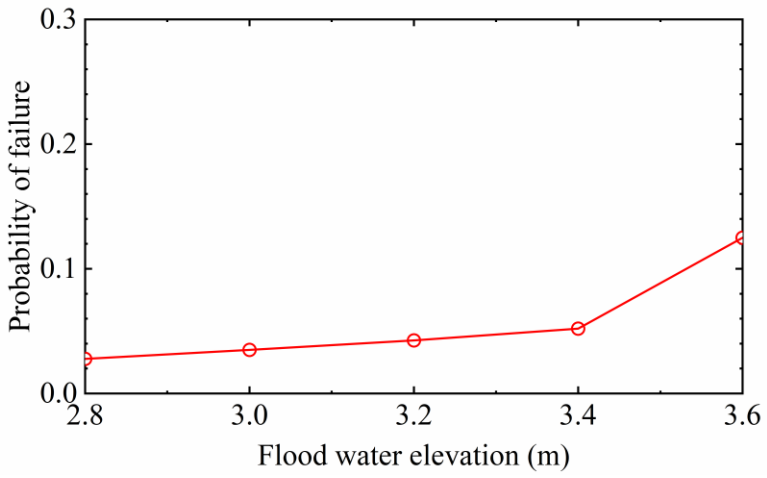

Figure 6. Effect of the flood water elevation on the probability of failure of the floodwall using random field method

4.2 Effect of the COV and scales of fluctuation of soil properties on the reliability of the floodwall using the random field method

To further investigate the influence of the uncertainties of the soil properties, a parametric study of COV and scale of fluctuation are performed for the reliability analysis of the floodwall. The probability of failure with different COV of clay soil and sand soil is illustrated in Figure 7 and Figure 8, respectively. Compared to the results from the random variable method, similar conclusions can be obtained from the random field method. For instance, a similar trend of the probability of failure with the flood water elevation can be found in Figure 7 and Figure 8. The probability of failure is varied with the flood water elevation at both low and high flood water elevations for the COV of the strength property of clay. The COV of the strength property of sand causes more effects on the probability of failure at high flood water elevations. However, it is interesting to find a lower probability of failure at high flood water elevations derived from the COV of the strength property of sand,

which is opposite to the conclusion from the random variable method. This can be explained that surrounding strong soil elements in the sand layer could resist the deformation triggered by the weak soil elements exactly around the pile tip, resulting in an "average" effect. In addition, as shown in Figure 9, the slip surface of the floodwall is formed in the clay layers rather than in the sand layer. The top layers are thick clay layers while the sand layer on the bottom of the floodwall system is thin in Figure 2, indicating that the COV of the strength property of clay layers will affect a larger area of the model domain in this example and is more likely to cause local weak soil zone. Therefore, the influence of the COV of the strength property of clay is more significant than that of the strength property of sand in the application of the random field method.

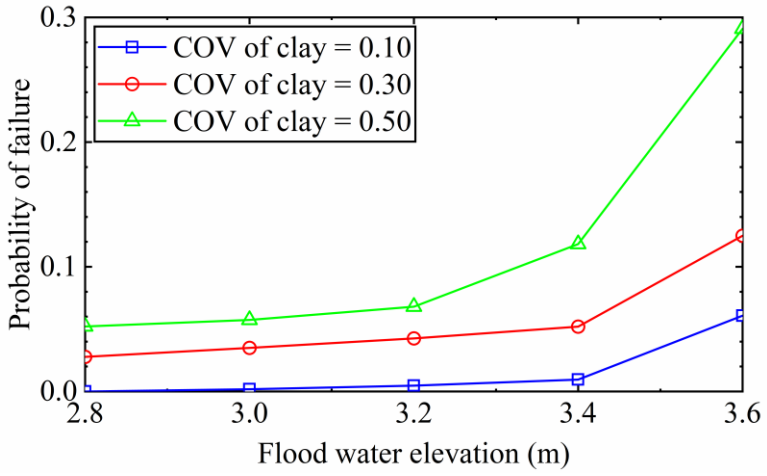

Figure 7. Effect of COV of the strength property of clay layers on the probability of failure of the floodwall using random field method

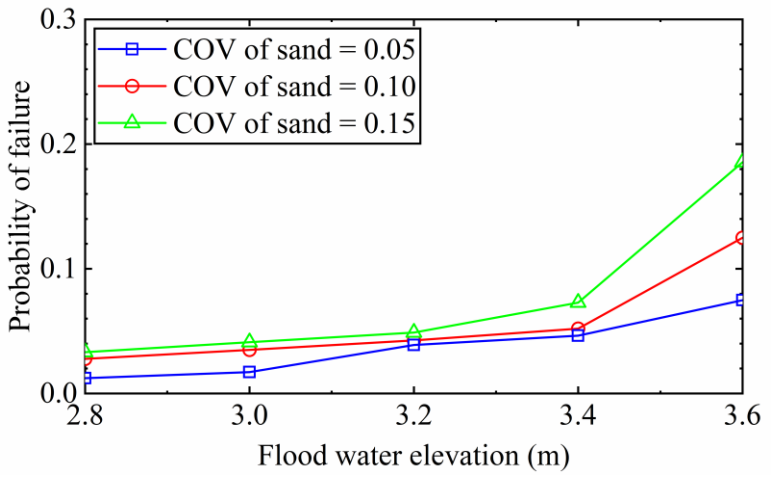

Figure 8. Effect of COV of the strength property of sand layer on the probability of failure of the floodwall using random field method

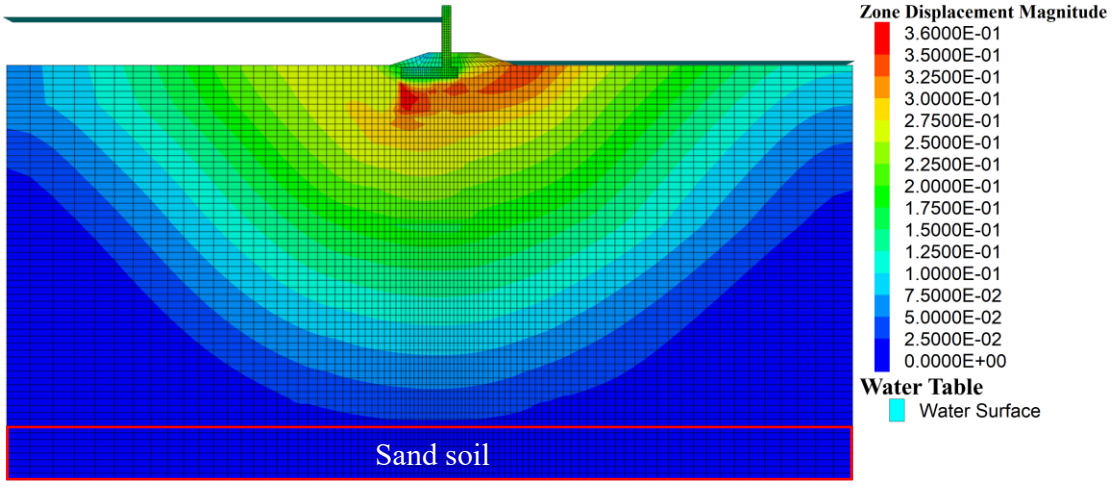

(a) Flood water elevation is 2.8 m

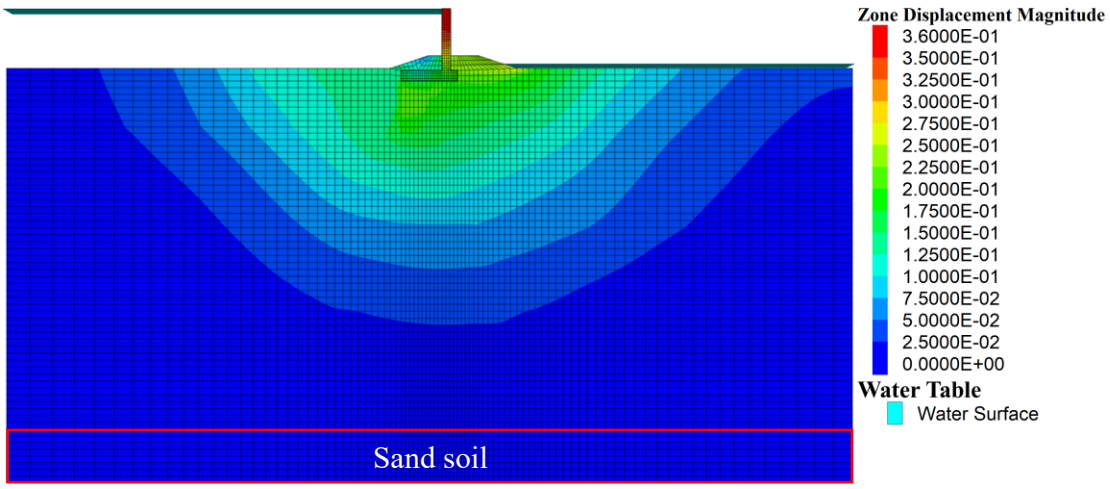

(b) Flood water elevation is 3.6 m

Figure 9. Contour of displacement of the floodwall with different flood water elevations in the deterministic analysis

Figure 10 and Figure 11 show the effect of the scales of fluctuation of the strength property of clay on the probability of failure. It can be found that the probability of failure increases with the horizontal and vertical scales of fluctuation λ_x and λ_y of the strength property of clay since large scales of fluctuation represent a higher correlation of soil properties and tends to cause local weak zones. The horizontal scale of fluctuation λ_x with a wider range causes a smaller effect on the probability of failure than λ_y, which agrees well with the results of the slope stability analysis in the previous studies (Cho 2010; Ji et al. 2012; Li et al. 2015). The ratio of the horizontal length to the vertical length of the numerical model is generally within an order of magnitude, which means the soil properties in the horizontal direction are highly correlated while that in the vertical direction can considerably fluctuate. Therefore, the influence of the λ_x on the probability of failure of the floodwall is more significant than λ_y. Similar conclusions can be found in Figure 12 and Figure 13 for the sand layer.

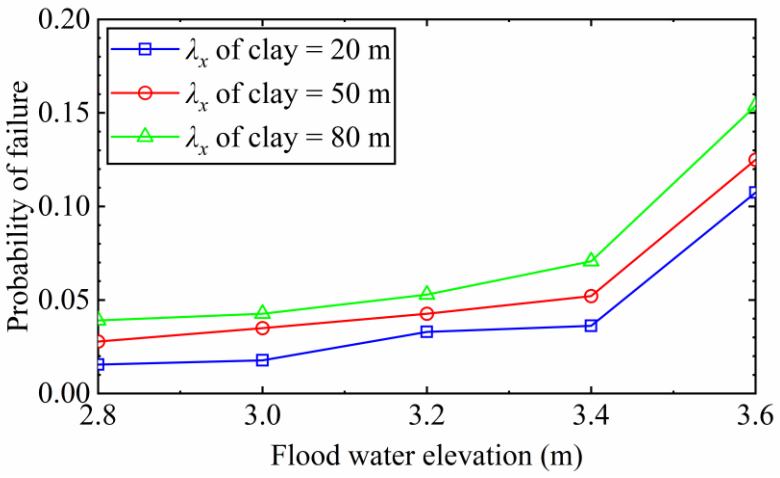

449

450 Figure 10. Effect of the horizontal scales of fluctuation of the strength property of clay layers
451 on the probability of failure of the floodwall using random field method
452

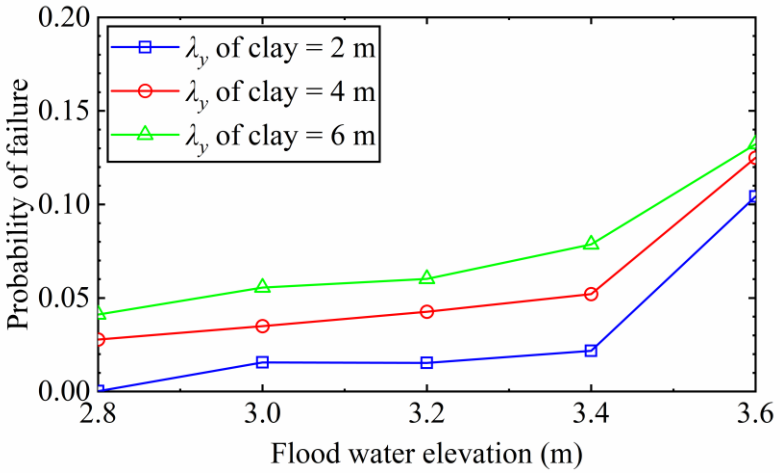

453

454 Figure 11. Effect of the vertical scales of fluctuation of the strength property of clay layers on
455 the probability of failure of the floodwall using random field method
456

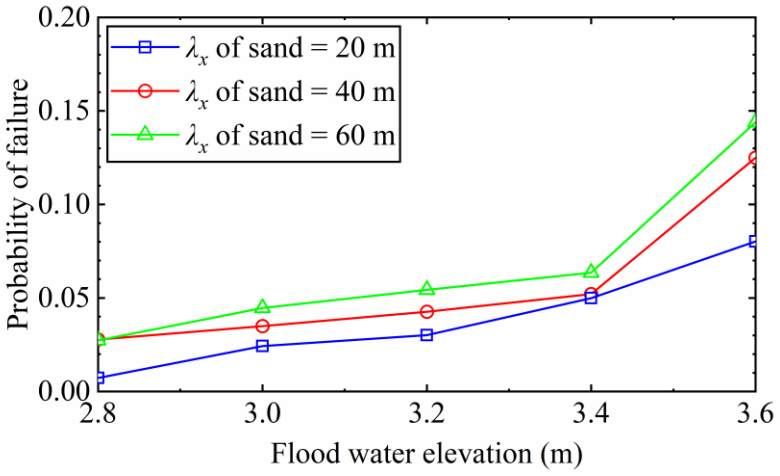

Figure 12. Effect of the horizontal scales of fluctuation of the strength property of sand layer on the probability of failure of the floodwall using random field method

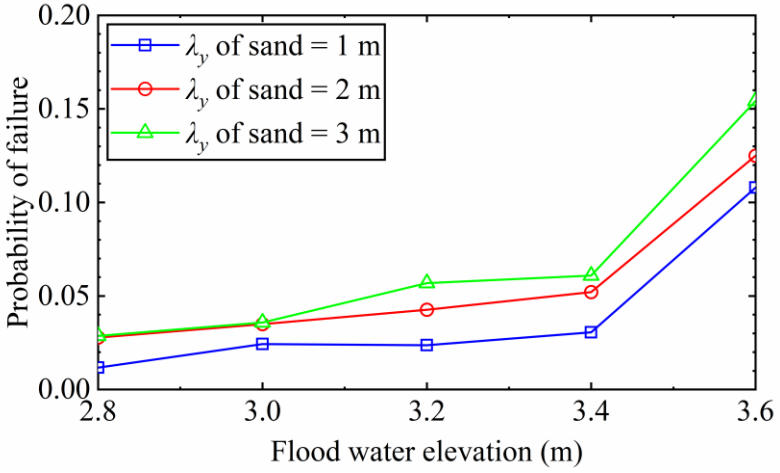

Figure 13. Effect of the vertical scales of fluctuation of the strength property of sand layer on the probability of failure of the floodwall using random field method

As is mentioned above, the random variable model is conceptually simple and can generally yield a more robust prediction of the geotechnical system response than the random field model. However, the random field model can rationally characterize the soil spatial variability and result in a more accurate prediction of the geotechnical system response. As such, it is crucial to know the similarities and differences between the random variable model

and random field model before a trade-off is made between the model robustness and model fidelity in the model selection for the reliability analysis of floodwalls. Figure 14 and Figure 15 present the comparison results of the two methods. For both two methods, the probability of failure increases with the COV of the strength property of clay for all flood water elevations and is sensitive to the COV of the strength property of sand at high flood water elevations. At low flood water elevations, the floodwall system is stable for both two methods and the probability of failure derived from RVM and RFM is at a similarly low level. The random variable method generally results in a higher probability of failure than the random field method at high flood water elevations, indicating that the RVM-based design could be more conservative without considering spatial variability of the soil properties in this case. The continuous slip surface can be easily formed when a weak soil element is sampled in one random variable simulation since the strength soil properties of all the soil elements in the model domain are the same as small in this simulation. By contrast, if a weak soil element is generated in one random field simulation, there could be strong soil elements in the model domain to prevent the extension of the slip surface and soil deformation around the pile tip due to the fluctuation of the soil properties. The “average” effect could be more obvious when the scale of fluctuation is small and make the results from the random field method close to the deterministic analysis results (Hicks et al. 2014). Note that the factor of safety *FS* in the deterministic analysis for all the flood water elevations in this study is greater than 1.0. It is reasonable to find that the probability of failure from the RVM is generally larger than that from RFM. Due to the “average” effect in the RFM, higher COV of the strength property of sand which determines the end bearing capacity of the H-piles will result in a lower probability of failure of the pile-founded floodwall than that from the RVM, since the strong

soil elements surrounding the weak soil elements exactly around pile tip will resist soil deformation at high flood water elevations. Although the sand layer is far from the slip surface and is thin at the bottom of the pile-founded T-wall, the uncertainties of the strength property of sand can also be crucial for the stability of the pile-founded T-wall, which is quite different from the layered slope stability analysis. The comparison results can provide some guidance for the model selection for the reliability-based floodwall designs, though many influencing factors (e.g., the economic benefits, time constraints, budget constraints, and geotechnical data availability) could be considered in the trade-off between the model robustness and model fidelity. For example, the random variable model can yield a larger probability of failure in this study, indicating that the designs based on the random variable method could be cost-inefficient in this case. When sufficient data can be available to calibrate the random field model, it is preferable to adopt the random field model to reach economic designs. If it is time-starved and well-budgeted, the designs based on the random variable method can be more acceptable since fewer field data are needed for accurate calibrations. It is also possible to combine the two models according to different design stages. In the initial stage of the design project, only limited field investigation data can be obtained and it is suitable to use the random variable method to give preliminary designs of the floodwall. As more data are available, these preliminary designs can be updated to be more economic designs using the random field method.

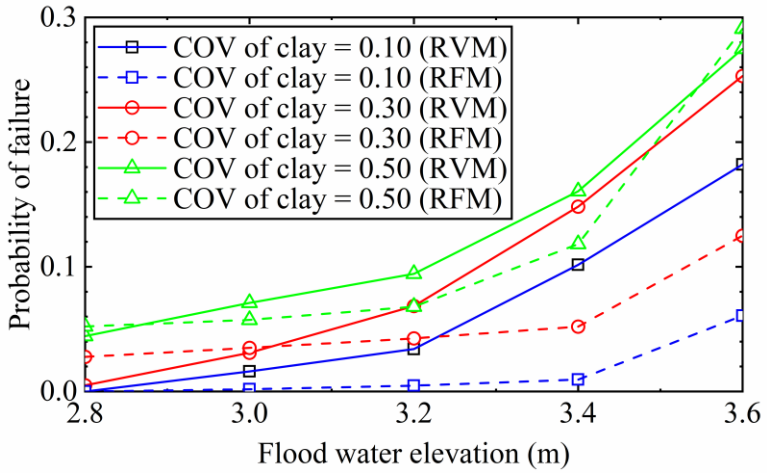

Figure 14. Comparison of COV of the strength property of clay layers between the results from random variable method and random field method

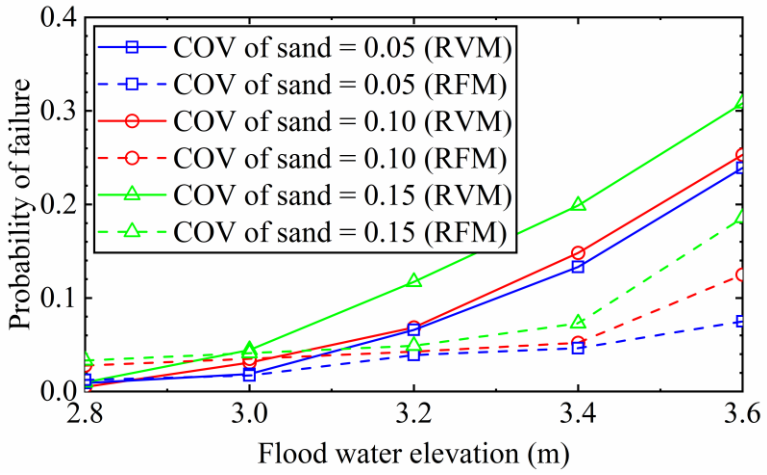

Figure 15. Comparison of COV of the strength property of sand layer between the results from random variable method and random field method

5. Summary and conclusions

This paper presents a comprehensive study to evaluate the reliability of the pile-founded T-wall system with several clay layers on the top and a sand layer on the bottom, where both the random variable method and random field method are used for the reliability analysis of the floodwall. The strength soil properties are modeled as random variables and

525 random fields, respectively. The parametric study is performed to investigate the effect of the
526 COV, and the horizontal and vertical scales of fluctuation (of the strength properties for clay
527 and sand) on the probability of failure. Based on the obtained results, the following
528 conclusions can be summarized.

529 1) For the random variable method, the probability of failure increases with the COV
530 of the strength properties for clay and sand. The probability of failure is less sensitive to the
531 COV of the strength property of sand at low flood water elevations.

532 2) For the random field method, the probability of failure increases with the COV and
533 (horizontal and vertical) scales of fluctuation of soil properties. The effect of the horizontal
534 scale of fluctuation is more profound than the vertical scale of fluctuation for clay and sand
535 layers.

536 3) The probability of failure derived from the random variable method is generally
537 higher than that from the random field method at high flood water elevations. The COV of the
538 strength property of sand is more likely to cause a large probability of failure than that of the
539 strength property of clay at high flood water elevations in the random variable method. By
540 contrast, the COV of the strength property of sand does the opposite in the random field
541 method, indicating that the COV of the strength property of clay is more influential on the
542 probability of failure than the COV of the strength property of sand in the random field
543 method.

544

545 **Acknowledgments**

546 The study on which this paper is based was supported partially by the National
547 Science Foundation through Grants 1818649 and 1900445. The results and opinions

548 expressed in this paper do not necessarily reflect the views and policies of the National
549 Science Foundation.
550
551 **References**

552 Adhikari, S., Song, C.R., & Cheng, A.H.D. (2014). Evaluation of I-wall in New Orleans with
553 back-calculated total stress soil parameters. *Acta Geotechnica*, 9(6), 1123-1134.
554 Alamanis, N. (2017). Uncertainties and optimization in geotechnical engineering. *American*
555 *Academic Scientific Research Journal for Engineering, Technology, and Sciences*, 38(1),
556 92-111.
557 Au, S.K., & Wang, Y. (2014). Engineering risk assessment with subset simulation. John Wiley
558 and Sons, Singapore.
559 Bodda, S. S., Gupta, A., Ju, B., & Kwon, M. (2019). Multi-hazard fragility assessment of a
560 concrete floodwall. *Reliability Engineering and Resilience*, 1(2), 46-66.
561 Chen, F., Zhang, R., Wang, Y., Liu, H., Böhlke, T., & Zhang, W. (2020). Probabilistic stability
562 analyses of slope reinforced with piles in spatially variable soils. *International Journal of*
563 *Approximate Reasoning*, 122, 66-79.
564 Cheng, H., Chen, J., Chen, R., & Chen, G. (2019). Comparison of modeling soil parameters
565 using random variables and random fields in reliability analysis of tunnel face.
566 *International Journal of Geomechanics*, 19(1), 04018184.
567 Cho, S.E. (2010). Probabilistic assessment of slope stability that considers the spatial
568 variability of soil properties. *Journal of Geotechnical and Geoenvironmental*
569 *Engineering*, 136(7), 975-984.
570 Davidson, M., Patev, R. C., & Consolazio, G. R. (2020). Probabilistic risk assessment of

barge impacts on hurricane floodwalls. *Journal of performance of constructed facilities*, 34(2), 04020010.

Fenton, G.A. (1994). Error evaluation of three random-field generators. *Journal of Engineering Mechanics*, 120(12), 2478-2497.

Gao, X., Liu, H., Zhang, W., Wang, W., & Wang, Z. (2019). Influences of reservoir water level drawdown on slope stability and reliability analysis. *Georisk: Assessment and Management of Risk for Engineered Systems and Geohazards*, 13(2), 145-153.

Gong, W., Juang, C.H., Martin, J.R., & Ching, J. (2016). New sampling method and procedures for estimating failure probability. *Journal of Engineering Mechanics*, 142(4), 04015107.

Gong, W., Juang, C.H., & Martin, J.R. (2017). A new framework for probabilistic analysis of the performance of a supported excavation in clay considering spatial variability. *Géotechnique*, 67(6), 546-552.

Gong, W., Tang, H., Juang, C.H., & Wang, L. (2020). Optimization design of stabilizing piles in slopes considering spatial variability. *Acta Geotechnica*, 15(11), 3243-3259.

Gong, W., Zhao, C., Juang, C. H., Zhang, Y., Tang, H., & Lu, Y. (2021). Coupled characterization of stratigraphic and geo-properties uncertainties–A conditional random field approach. *Engineering Geology*, 294, 106348.

Hasofer, A.M., & Lind, N.C. (1974). Exact and invariant second-moment code format. *Journal of the Engineering Mechanics Division*, 100(1), 111-121.

Hicks, M.A., Nuttall, J.D., and Chen, J. (2014). Influence of heterogeneity on 3D slope reliability and failure consequence. *Computers and Geotechnics*, 61, 198-208.

Hu, J., Makdisi, F., Wang, Z.L., Hokens, K., & Schwanz, N. (2013). Three Dimensional

Soil-Structure-Interaction Analysis of a Flood Wall Under Full-Scale Load Test. *Seventh International Conference on Case Histories in Geotechnical Engineering*.

Hu, J. Z., Zheng, J. G., Zhang, J., & Huang, H. W. (2023). Bayesian Framework for Assessing Effectiveness of Geotechnical Site Investigation Programs. *ASCE-ASME Journal of Risk and Uncertainty in Engineering Systems, Part A: Civil Engineering*, 9(1), 04022054.

Huang, J., Fenton, G., Griffiths, D.V., Li, D., & Zhou, C. (2017). On the efficient estimation of small failure probability in slopes. *Landslides*, 14(2), 491-498.

Huang, J., and Griffiths, D.V. (2015). Determining an appropriate finite element size for modeling the strength of undrained random soils. *Computers and Geotechnics*, 69, 506-513.

Huang, L., Huang, S., & Lai, Z. (2020). On the optimization of site investigation programs using centroidal Voronoi tessellation and random field theory. *Computers and Geotechnics*, 118, 103331.

Itasca Consulting Group, Inc. (2022). FLAC3D - Fast Lagrangian Analysis of Continua in 3 Dimensions, Version 7.0. Minneapolis, MN.

Ji, J., Liao, H.J., & Low, B.K. (2012). Modeling 2-D spatial variation in slope reliability analysis using interpolated autocorrelations. *Computers and Geotechnics*, 40, 135-146.

Jiang, S.H., Li, D.Q., Zhang, L.M., & Zhou, C.B. (2014). Slope reliability analysis considering spatially variable shear strength parameters using a non-intrusive stochastic finite element method. *Engineering Geology*, 168, 120-128.

Jiang, S.H., & Huang, J.S. (2016). Efficient slope reliability analysis at low-probability levels in spatially variable soils. *Computers and Geotechnics*, 75, 18-27.

Juang, C.H., Gong, W., & Martin, J.R. (2017). Subdomain sampling methods - Efficient

algorithm for estimating failure probability. *Structural Safety*, 66, 62-73.

Juang, C.H., Gong, W., Martin II, J.R., & Chen, Q. (2018). Model selection in geological and geotechnical engineering in the face of uncertainty-does a complex model always outperform a simple model? *Engineering Geology*, 242, 184-196.

Knabe, W., Przewłócki, J., & Różyński, G. (1998). Spatial averages for linear elements for two-parameter random field. *Probabilistic Engineering Mechanics*, 13(3), 147-167.

Li, D.Q., Jiang, S.H., Cao, Z.J., Zhou, W., Zhou, C.B., & Zhang, L.M. (2015). A multiple response-surface method for slope reliability analysis considering spatial variability of soil properties. *Engineering Geology*, 187, 60-72.

Link, L. E. (2021). How Hurricane Katrina influenced the design of hurricane protection and risk reduction systems and national approaches to risk and resilience: Part 1. Hurricane Katrina and New Orleans: A forensic assessment, risk and reliability analysis, and key lessons learned. *Water Policy*, 23(S1), 156-173.

Lo, M. K., & Leung, Y. F. (2017). Probabilistic analyses of slopes and footings with spatially variable soils considering cross-correlation and conditioned random field. *Journal of Geotechnical and Geoenvironmental Engineering*, 143(9), 04017044.

Ma, G., Rezania, M., & Nezhad, M.M. (2022). Effects of spatial autocorrelation structure for friction angle on the runout distance in heterogeneous sand collapse. *Transportation Geotechnics*, 33, 100705.

Phoon, K.K., & Kulhawy, F.H. (1999). Characterization of geotechnical variability. *Canadian Geotechnical Journal*, 36(4), 612-624.

Rajabalinejad, M., van Gelder, P.H.A.J.M., Demirbilek, Z., Mahdi, T.F., & Vrijling, J.K. (2010). Application of the dynamic bounds method in the safety assessment of flood

defences, a case study: 17th street flood wall, New Orleans. *Georisk*, 4(4), 157-173.

Rajabalinejad, M., & Demirbilek, Z. (2011). Safety assessment of infrastructures using a new Bayesian Monte Carlo method. *Georisk: Assessment and Management of Risk for Engineered Systems and Geohazards*, 5(3-4), 195-206.

Ravichandran, N., Wang, L., & Rahbari, P. (2022). Robust Optimization for Stability of I-Walls and Levee System Resting on Sandy Foundation. *KSCE Journal of Civil Engineering*, 26(1), 57-68.

Spencer, W.A. (2007). Parallel stochastic and finite element modeling of clay slope stability in 3D. The University of Manchester (United Kingdom).

USACE (2012). Hurricane and Storm Damage Risk Reduction System Design Guidelines, INTERIM, New Orleans District Engineering Division, U.S. Army Corps of Engineers. New Orleans, LA

Wang, L., Wu, C., Tang, L., Zhang, W., Lacasse, S., Liu, H., & Gao, L. (2020). Efficient reliability analysis of earth dam slope stability using extreme gradient boosting method. *Acta Geotechnica*, 15, 3135-3150.

Wang, Y., Cao, Z., & Au, S. K. (2010). Efficient Monte Carlo simulation of parameter sensitivity in probabilistic slope stability analysis. *Computers and Geotechnics*, 37(7-8), 1015-1022.

Won, J., Adhikari, S., Song, C.R., Cheng, A.H.D., & Al-Ostaz, A. (2011). Evaluation of a T-wall section in New Orleans considering 3D soil-structure interaction. *Journal of Geotechnical and Geoenvironmental Engineering*, 137(8), 731-742.

Wu, Y., Zhou, X., Gao, Y., Zhang, L., & Yang, J. (2019). Effect of soil variability on bearing capacity accounting for non-stationary characteristics of undrained shear strength.

Computers and Geotechnics, 110, 199-210.

Yun, W., Lu, Z., He, P., Dai, Y., & Feng, K. (2020). Adaptive subdomain sampling and its adaptive Kriging–based method for reliability and reliability sensitivity analyses. *Structural and Multidisciplinary Optimization*, 61(3), 1107-1121.

Zhang, W. G., Meng, F. S., Chen, F. Y., & Liu, H. L. (2021). Effects of spatial variability of weak layer and seismic randomness on rock slope stability and reliability analysis. *Soil Dynamics and Earthquake Engineering*, 146, 106735.

Lists of Tables

Lists of Figures